URTeC: 3864551

Integrated Workflows for Drilling Optimization and Enhanced Production

Jakob Heller[1], Venkatesh Anantharamu*[1], Andrew Lewis[2], and Ron Bianco[3],
1. Ikon Science Americas Inc., 2. Fairfield Geotechnologies,
3. Fasken Oil and Ranch, ltd.

Abstract

Accurate pore pressure and stress estimation are extremely important for safe and efficient drilling. The objective of this study is to establish robust models for an unconventional shale play to predict pore pressure and stress magnitudes from elastic properties derived from seismic. The pore-pressure magnitudes have often been shown to impact productivity and minimum horizontal stress (Shmin) link directly to 'fraccability' of a rock.

Introduction

Unexpected overpressure is a major cause of drilling hazards, costing the industry billions of dollars and posing a huge potential risk for damage to the environment. Overpressure also has a significant impact on the ability to artificially fracture shale formations as well as increasing the production drive of liquid hydrocarbons and favor higher production rates. The derived volumes of pore pressure and stress can assist in determining "sweet spots" within a play.

To derive the 3D pore-pressure and geomechanical properties, seismic data is crucial. In this case, the data was acquired using high trace density seismic acquisition. This improved the spatial resolution of the seismic and its associated seismic attributes. This enabled the interpretation of structural and stratigraphic geologic frameworks that are less resolved using onshore acquisition methods typical for the late-2000s. The survey geometry collected additional data such as acquisition of more near and far offset traces, finer lateral sampling, higher fold, broader frequencies, and fuller azimuthal sampling. All of these increased the resolution that illuminated fine-scale geology.

Using the above seismic data, we have done an integrated study involving phases 1 and 2. As part of phase 1, a detailed petrophysics and rock physics analysis was performed, then seismic AVO conditioning and finally, seismic AVO inversion was performed to extract elastic properties from seismic angle stacks. Parallelly in phase 2, a detailed pore pressure and geomechanics analysis was performed on a series of wells throughout the study area. 1D calibrated models for pore pressure estimation, stress and failure were

constructed based on detailed drilling history reviews of offset wells, formation pressures and fracture closure pressures from DFITs, Image log data and lab rock mechanical tests. Finally, both the phases were combined to estimate the properties in 3-dimensions.

The dataset used is in the Midland Basin, which is the eastern part of the Permian Basin as shown in Figure 1. The stratigraphy of the Basin is widely characterized as multilayer stacked geological zones with unique sedimentary features. These stacked plays along with high fracture rates are the primary reasons the Midland Basin has great potential for hydrocarbon recovery.

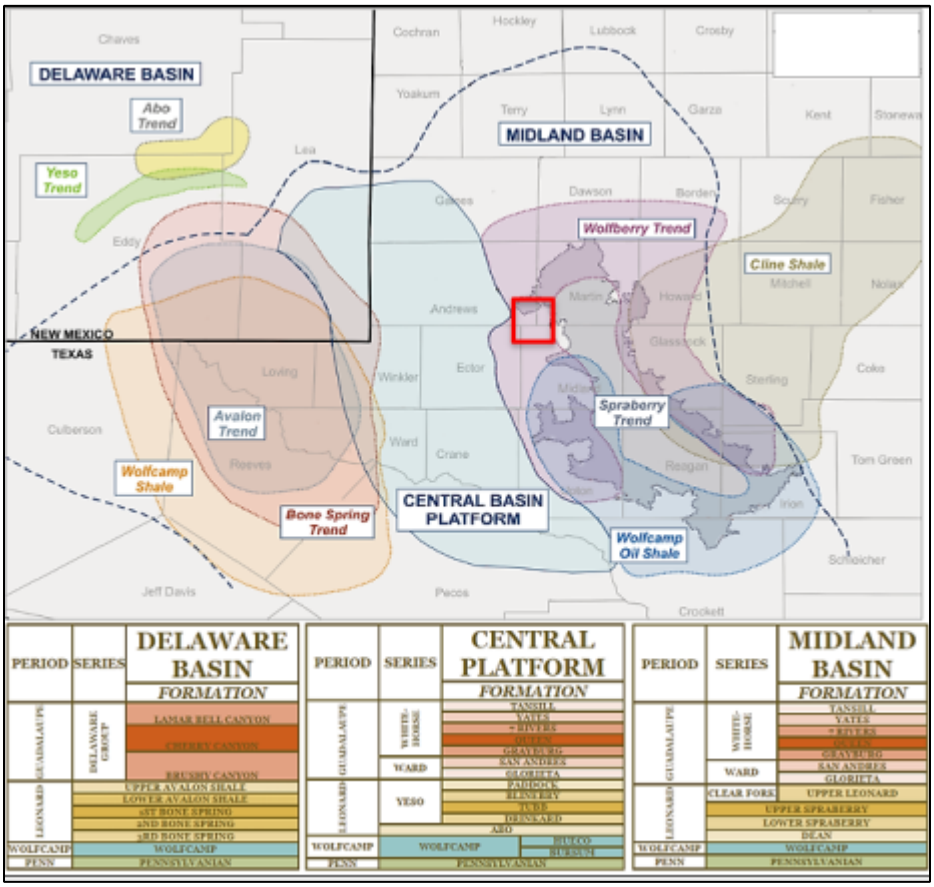

Figure 1. Map of the Permian Basin with the study area highlighted in the red square. Image modified from Green et al., 2018.

Stresses and Overpressure in the Permian Basin – Previous work

Overpressure in the Permian Basin has been attributed to various mechanisms. Swarbrick (1995), Sinclair (2007) and Van Der Loop (2019) have argued that overpressure in the Delaware Basin, which can be in excess of 8000 psi, mainly was caused by disequilibrium compaction with possible minor additional overpressure due to gas generation in sections deeper/older than the Wolfcamp series. Other authors (e.g., Luo et al., 1994) argued for a combination of mechanisms (e.g., disequilibrium compaction, aquathermal and hydrocarbon generation). Xiong et al., (2015) reported pressure gradients in the Wolfcamp series between 0.55 psi/ft – 0.75 psi/ft, while Loughry et al., (2015) from an extensive study reported pressure gradients in the Wolfcamp B in the Midland Basin between 0.5 psi/ft – 0.6 psi/ft. They argued for a correlation between elevated pressure gradients and areas of high(er) thermal maturity. Friedrich and Monson (2013) reported average pressure gradients in the Wolfcamp between 0.61 psi/ft and 0.66 psi/ft.

In the Midland Basin, the Spraberry, or parts of the Spraberry, has been reported to be underpressured possibly related to production or perhaps uplift (e.g. Loughry et al., 2015).

A dataset of about 25 wells from the Midland Basin was available for this study with a detailed analysis performed on a subset of wells with available lab rock mechanics test data available for model calibration.

Methods

High Trace Density (HTD) Acquisition and Processing

The 3D surface seismic data used in this study is well-sampled. In terms of trace density, or number of traces within a given area, this survey collects about 16.7 million traces per square mile. These data are collected in different domains that benefit both vertical and lateral resolution of the 3D seismic volume. This additional information includes (Lewis et al., 2021):

- Fine sampling of both near and far offsets
- Fine lateral sampling
- High fold
- Broadband vibroseis sweep
- Full azimuthal sampling

In general, the acquisition parameters of this HTD 3D survey collect a dense sampling of the full offset range at all azimuths, with a focus on collecting near offsets (Figure 2). The near offsets are collected by using 495' source and receiver line spacings combined with 82.5' (dual source lines) source station intervals and 165' receiver station intervals. These data are binned at 41.25' x 41.25' with a nominal fold of 1024. By comparison, typical surface seismic in the Permian Basin at the time this survey was acquired (2019) is binned at 82.5' x 82.5' with a nominal fold of 400. The trace density of HTD surface seismic designs is approximately ten times denser, creating a step change in the quality of onshore 3D surface seismic (Figure 3).

Furthermore, HTD acquisition design enables a more robust implementation of the seismic processing and imaging toolkit. Picking first breaks on the near offset traces more accurately measures refractor velocity variability in the near-surface weathering layer. Denser acquisition of near offsets and a broadband sweep better resolve surface waves characterized by low velocity and low frequency. This benefits ground roll noise attenuation techniques that model and subtract ground roll from the seismic data. Velocity analysis becomes much more stable, especially in the shallower formations. Even post-migration processes such as measuring the Velocity Variation with Azimuth (VVAz) are not biased by difference in inline or crossline offset. These data are collected with full azimuth out to three miles of inline and crossline offset. Angle stacks are generated every eight degrees from zero to forty-eight degrees. Each angle stack contains an incredible amount of detail due to the trace density of these data (Figure 4).

The benefits of the acquisition design and processing sequence go hand-in-hand with the quantitative interpretation workflow. The tighter source and receiver line spacings greatly benefit shallow resolution as well as lateral resolution. The trace density going into each of the angle stacks benefits the signal-to-noise ratio which effectively increases vertical resolution by lowering the noise floor of the seismic spectrum. This uplift in spatial resolution enables the analysis of seismic-derived rock properties at a finer-scale.

Vintage:	2019
CDP Bin Dimensions:	41.25' x 41.25'
Nominal Fold:	1024
Record Length:	6 seconds
Source Interval:	82.5' (dual source lines)
Sources per square mile	1370
Source Line Spacing:	495'
Number vibs	2
Sweeps per Vibrator Point:	1
Sweep Bandwidth:	2-92 Hz
Sweep Length:	24 seconds
Linear or Nonlinear Sweep:	Nonlinear | Low Dwell
Receiver Interval:	165'
Receiver Line Spacing:	495'
Receivers per square mile	342
Recording Geometry (lines x channels):	64 X 192 = 12,288
Recording Swath Dimensions:	15,840' X 15,840'
Off Diagonal (maximum offset)	22,401'
Trace Density per square mile	16,777,216

Figure 2. C-Ranch HTD 3D Seismic Acquisition Parameters

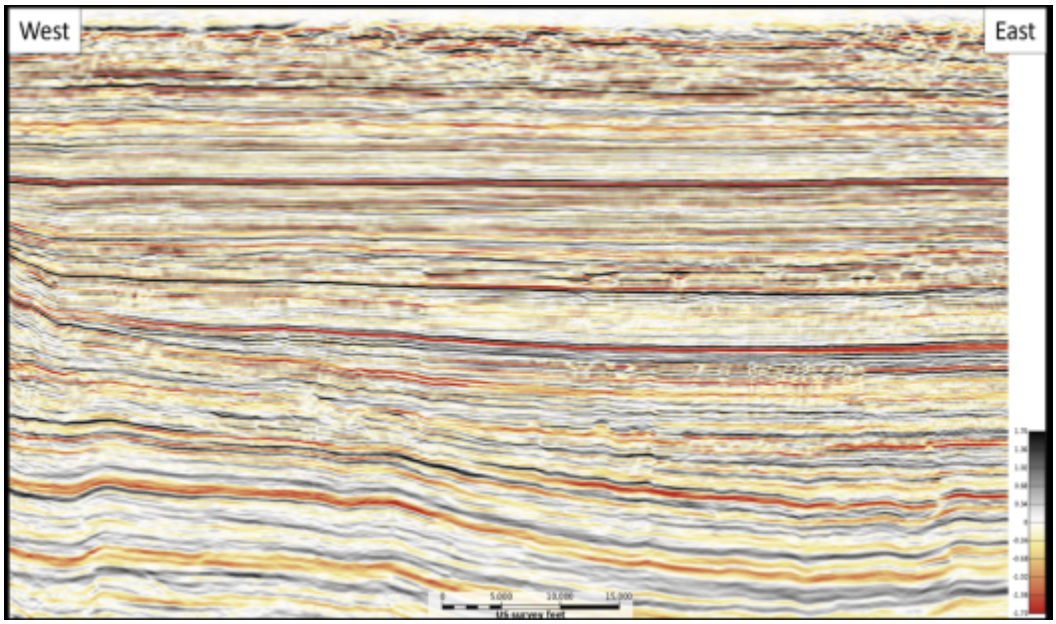

Figure 3. Central Basin Platform into Midland Basin: West – East line of C-Ranch PSTM Full Stack

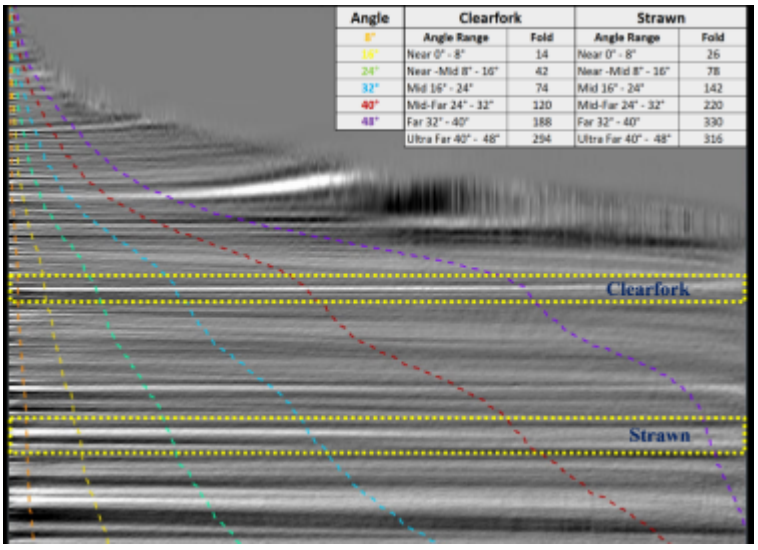

Angle	Clearfork		Strawn	
	Angle Range	Fold	Angle Range	Fold
8°	Near 0° - 8°	14	Near 0° - 8°	26
16°	Near -Mid 8° - 16°	42	Near -Mid 8° - 16°	78
24°	Mid 16° - 24°	74	Mid 16° - 24°	142
32°	Mid-Far 24° - 32°	120	Mid-Far 24° - 32°	220
40°	Far 32° - 40°	188	Far 32° - 40°	330
48°	Ultra Far 40° - 48°	294	Ultra Far 40° - 48°	316

Figure 4. Gather with angles overlaid and estimated fold per angle stack at both Clearfork and Strawn events

Seismic Data Conditioning

Seismic data processing is normally targeted for recovery of correct relative amplitudes and imaging. The same data may not be best suited for AVO analysis. For inversion/AVO analysis, it is necessary to condition the data accordingly. The goal of this workflow was to make seismic amplitudes proportional to the synthetic model calculated from the elastic impedances.

The Structure Oriented Filtering (SOF) was used to remove unwanted noise (mostly high frequency) from seismic data whilst preserving the signal. A dip-estimate was made from the mid-stack volume using a dip-scanning technique based on XCC of trace within a specific kernel type. In Midland Basin, which has a structurally complex sedimentary basin with an extensive history of tectonic deformation (Bhatnagar et. al., 2019), care must be taken to not overly smooth and make sure the geological features are preserved. For example, Figure 5 shows Mass Transport Deposits in the Upper Leonard interval (Lower Permian) and the corresponding calculated dip volume shows these geological variations being preserved. The near and near-mid stacks had relatively higher noise compared to all other stacks and hence a stronger filter was applied to them compared to the rest.

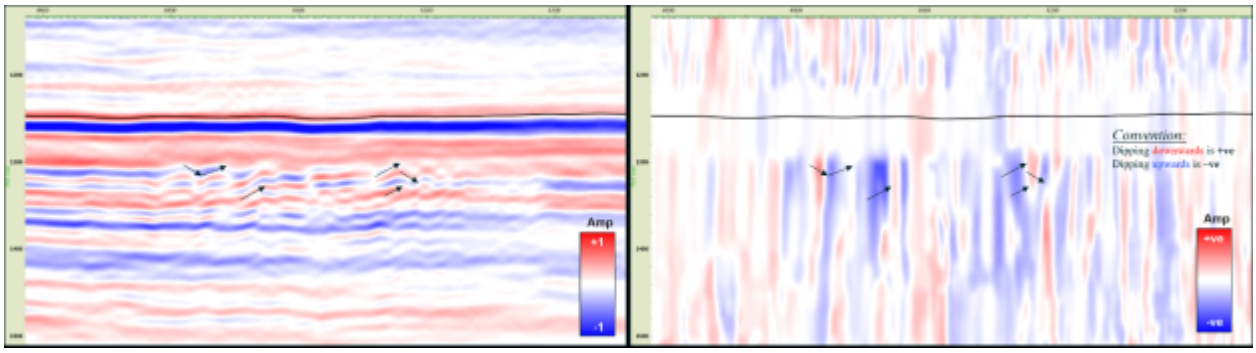

Figure 5. Mid stack volume with MTDs shown in arrows (left), dip volume on the same inline which shows geological features such as MTDs are being preserved.

A Frequency Slice Filtering was used suppress the noise in the lower frequency spectrum below 15Hz. De-noising was performed based on noise considerations by running a smoothing filter on a block of data in which the size of the block was determined by calculating the average post-migration Fresnel zone radius for each frequency. The low-frequency noise was minimal in all the stacks, however, the filtering did show improvements in the data.

As we know, the frequency of seismic data generally decreases with increasing offset with the effect primarily related to the application of moveout correction to hyperbolic reflections. Spectral balancing step was performed to reduce the effects of frequency loss due to increased transmission distance in far offsets and NMO stretch. The overarching goal – as with all processes in seismic data conditioning workflows was to improve consistency of output wavelets across the angle range.

A Taylor Time Shift (TTS) method was then applied to the data to remove residual moveout across the partial angle stacks. The method employs a least squares solution to the first order Taylor expansion for estimating time shifts among two or more volumes simultaneously. Care must be taken to preserve the AVO characteristics. Hence, synthetic pseudo-gathers were calculated around wells that showed the effect of AVO we should expect from seismic. Using that as a reference, time alignment was calculated based on TTS (Figure 6).

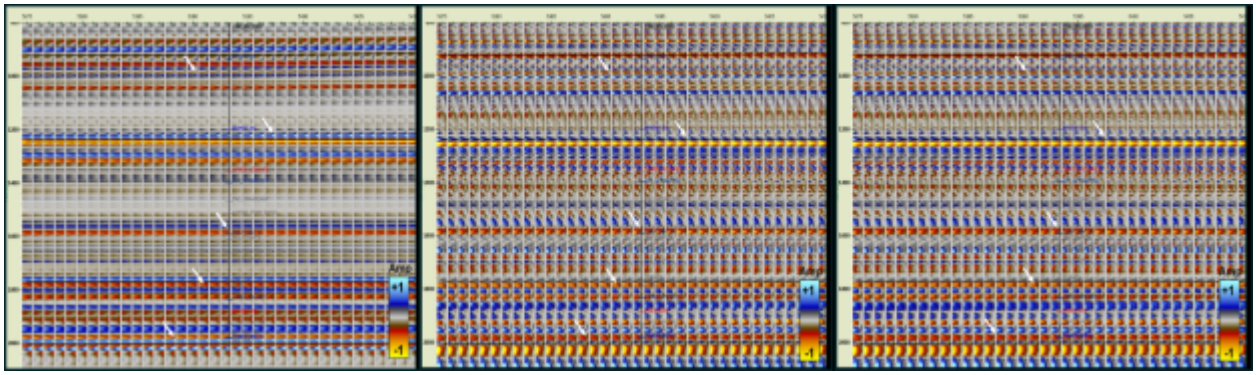

Figure 6. Synthetic psuedo-gathers calculated around a well and AVO characteristics that needs to be preserved are shown in arrows (left), seismic pseudo-gathers from angle stacks before TTS (middle), seismic after TTS (right).

Regarding lateral amplitude corrections, it was not evident that any surface related geology affected the amplitudes in any formations. We did some corrections at the edges and places where there were missing data. Finally, seismic scaling was done to scale the relative amplitudes of the angle stacks to the scale of AVO profiles computed from the wells. A single bulk scaling factor was calculated for all the formations.

Seismic Inversion

Ji-Fi (Joint Impedance and Facies Inversion), which is a Bayesian based inversion that solves simultaneously for elastic properties and facies (Kemper & Gunning, 2014) from multiple partial angle stacks was used in this case. Geological facies were grouped based on their elastic separation with each formation. Facies dependent depth/time trends (Figure 7) were built to parameterize the expected variability in elastic properties. Given the small interval over which these facies exist and that there is very little compaction effect seen in the facies, a constant value was the best option. Each trend is calculated with an accompanying estimate of the uncertainty. The calculated trends were used to construct a series of probability density functions (PDFs) in the elastic cross plot domains (Figure 7). The constant TWT:Vp trend defines a point in elastic space. The shape of the uncertainty ellipse is subsequently defined by the Vp:Rho, Vp:Vs trends plus uncertainties.

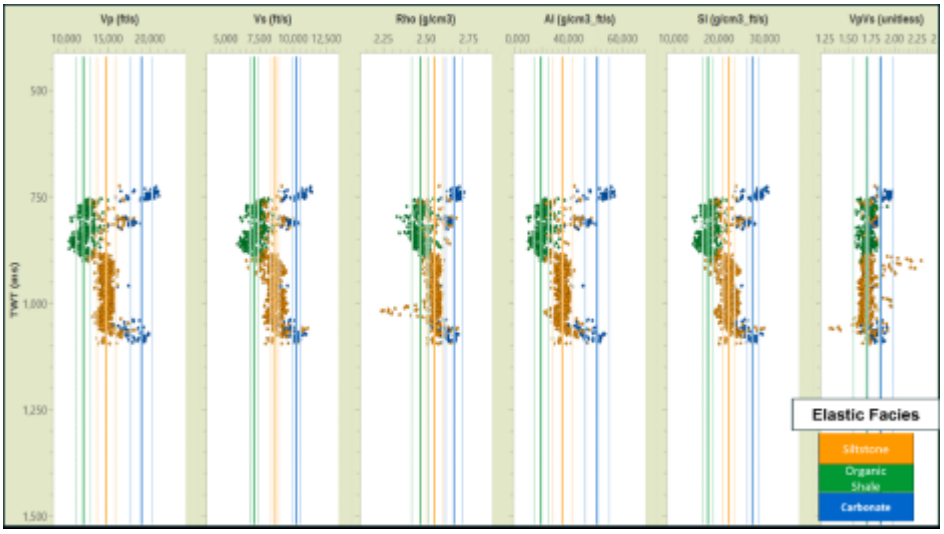

Figure 7. Depth/time-based trends are shown per facies by the solid line, the light lines express the uncertainty as 1 standard deviation for the Spraberry formation of Midland Basin.

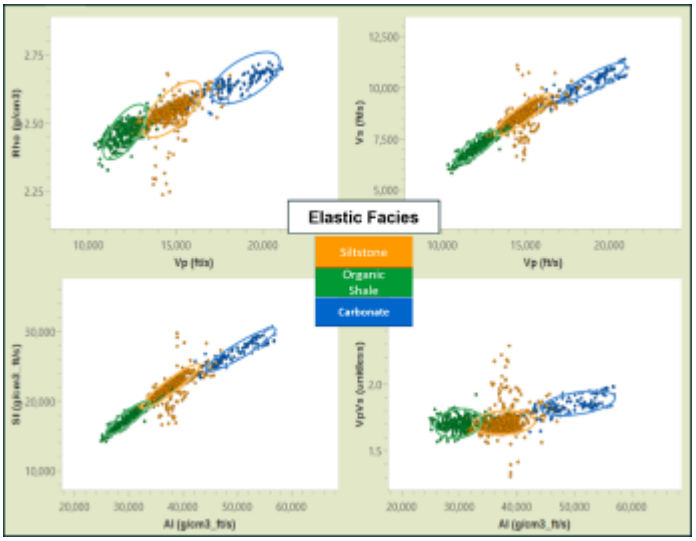

Figure 8. The distributions are shown for each facies in various elastic spaces for Spraberry formation. Each ellipse represents 1 standard deviation spread, i.e., 68% of the data. Note that these are not true PDFs as they do not have a height.

1D calibrated geomechanical model

A calibrated 1D geomechanical model was developed from available well and core laboratory data. The objective of a 1D geomechanics calibration is to develop a calibrated mechanical model of the well (meaning stresses, pore pressure, and rock mechanics properties) and then to 'drill the well on paper' so the mud pressures used in reality may be applied to the well with the objective of re-producing the geomechanics-related events (kicks, losses, breakouts etc.) that were observed when the well was drilled in reality. The calibrated mechanical model may then be applied, for example to well planning or completions planning.

Note that significant information is used for 1D analysis: drilling and completions history, log data, field pressure measurements, lab rock mechanics test results. High quality data typically leads to better calibrations and greater certainty for well and field planning. The 1D geomechanical workflow is shown in Figure 9 below.

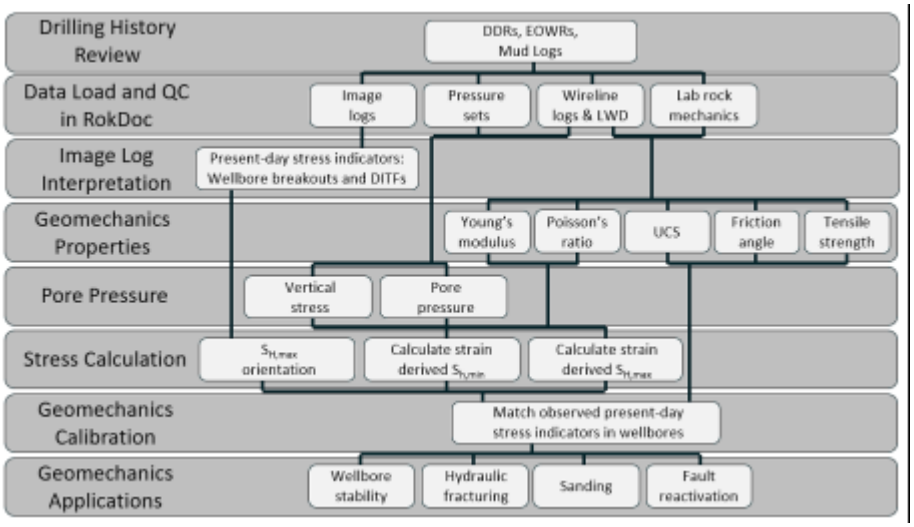

Figure 9. 1D Geomechanical workflow is shown from top to bottom.

Pore pressure in the study wells was predicted using two different models; a so-called "Pressure Reference Trend" (PRT) model and a rock physics constrained model (see Anantharamu et al., 2021 for detailed description). In our analysis, we utilized log data (Vp) corrected for TOC to optimize the final pore pressure estimates (Figure 10).

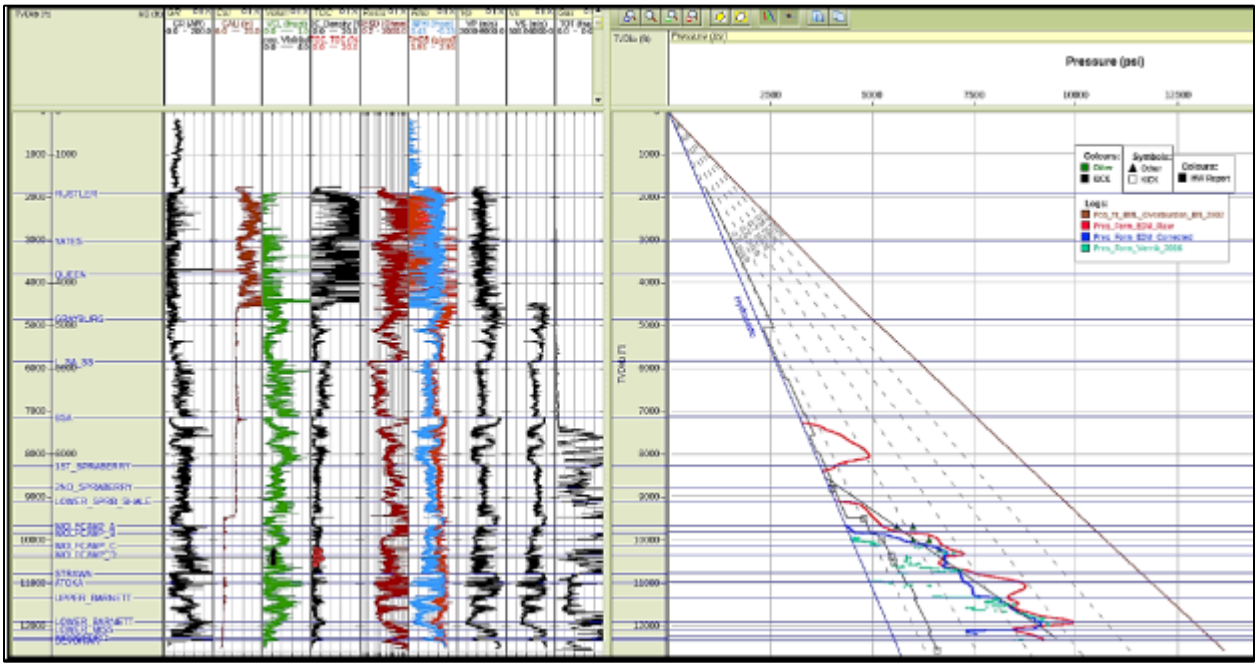

Figure 10. Pressure-depth plot well A from the Midland Basin. In the plot are displayed mud weight and kick data and digitized pressure data point from the Wolfcamp Formation (Friedrich and Monson, 2013). A regional pressure trend from DFIT data is also shown in black. Shale pressure has been predicted using equivalent depth method and raw (red) and TOC corrected (blue) Vp log data. Pore pressure was also predicted using Vernik (2016). The pore pressure profiles broadly agree and indicate underbalanced drilling from Lower Spraberry Shale to TD of the well. Note the indicated pressure regression near top Devonian from the Vclay and TOC corrected Vp log prediction (blue curve).

Laboratory rock mechanics test results have been interpreted to determine the mechanical properties most relevant to geomechanics analysis (Young's modulus and Poisson's ratio; unconfined compressive strength and internal friction angle; tensile strength). Correlations between well sonic Vp and rock mechanical properties measured in the lab have been developed. Overall, the shear strength of these Midland Basin 'gas shale' formations is not well represented by a single published model (Figure 11).

A)

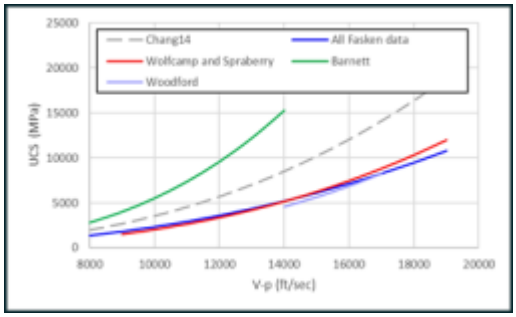

B)

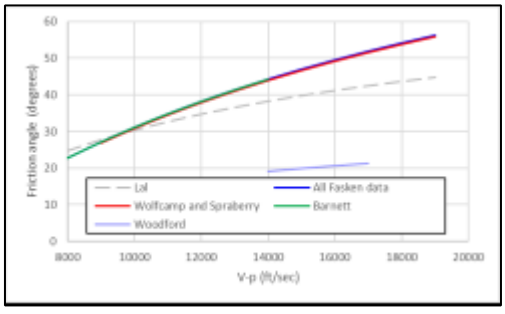

Figure 11. Correlations between well sonic Vp and rock mechanical properties measured in the lab were developed. As can be seen in the diagrams above, the shear strength of these Midland Basin 'gas shale' formations is not well represented by a single published model so that shear strength parameters have separate values for different formations.

Principal horizontal stress orientations are inferred from present-day stress indicators (wellbore breakouts and drilling-induced tensile fractures) in image logs and from regional information. Analyzed image log data indicate an azimuth of SHmax of 079°, which is within a few degrees of that reported by Lund Snee and Zoback (2018). Typically, 075°.

The horizontal stress magnitudes are calculated at all depths in all calibration wells using the poroelastic strain equations, which take into account all geomechanics information obtained to this point: vertical stress (Sv), pore pressure (Pp), elastic modulus (E), and Poisson's ratio (ν), plus Biot coefficient (α) derived for each Formation from measured elastic moduli and calculated mineral modulus (0.65 – 0.8) and the poroelastic strain magnitudes (eh,min, eH,max). The final values of eH,max and eh,min are determined by calibrating predicted wellbore breakouts and DITFs to present-day stress indicators interpreted from image logs. The predicted stress profiles are characteristic of a strike-slip stress regime through most of the logged interval except in a few intervals (usually Spraberry or parts of Wolfcamp) in which they are normal faulting stress regime (Figure 12).

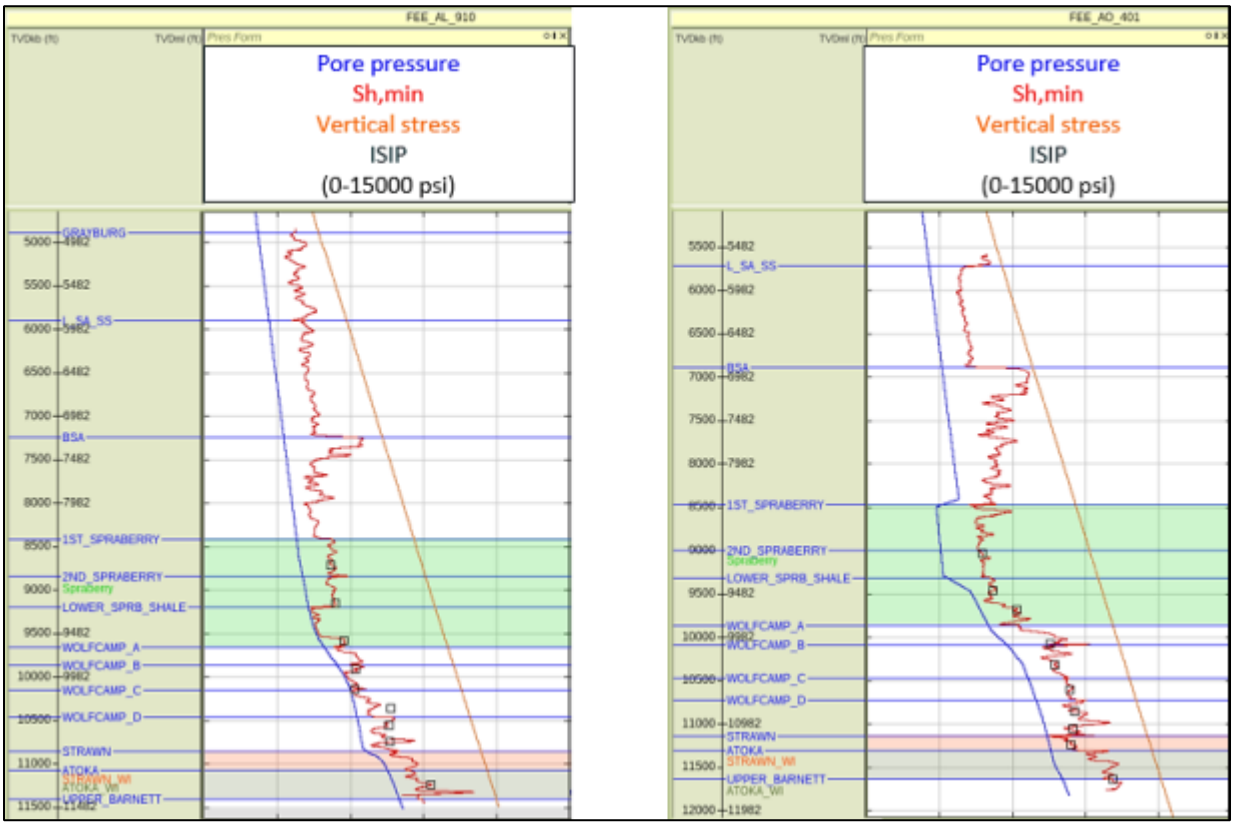

Figure 12. Correlations between well sonic Vp and rock mechanical properties measured in the lab were developed. As can be seen in the diagrams above, the shear strength of these Midland Basin 'gas shale' formations is not well represented by a single published model so that shear strength parameters have separate values for different formations.

Results

As Ji-Fi does not use conventional approach of static low-frequency model building, there is no bias added from the well data/locations. Hence, every single well would be a true blind test. Here is an example well (Figure 13) which shows comparison of up-scaled elastic properties measured at the well and the inverted properties from the seismic. We can see very good correlations between the two. The residuals show a ringing effect which is caused by inter-carbonate multiples in the shallow formations and the inversion algorithm has taken out these amplitudes and were not used for the predictions.

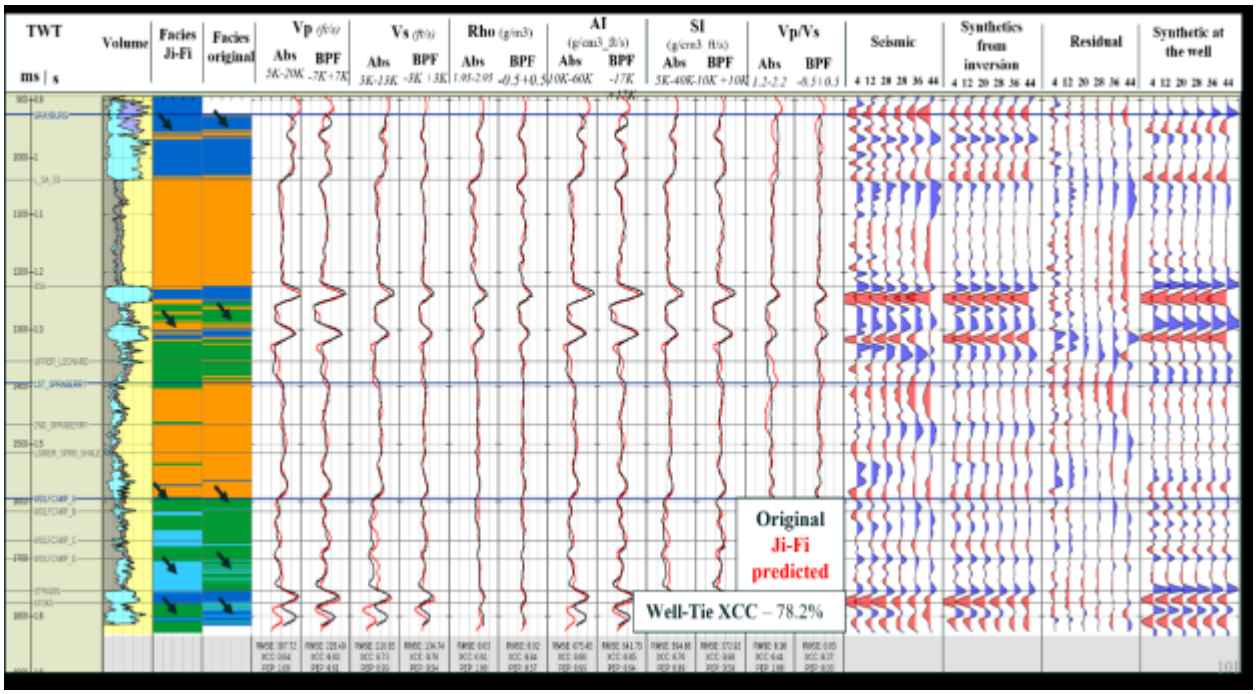

Figure 13. Inversion results at a well showing comparison of elastic properties measured and predicted.

Figure 14 shows the conditioned seismic, predicted facies & acoustic impedance from the inversion on an inline. The lateral continuity of the facies and elastic properties are controlled by the seismic reflectivity alone unlike conventional model-based inversion approaches, no lateral interpolation of well log data is used in this case. Hence, this methodology is ideally suited for mapping the discontinuous and complex geology of the Midland Basin.

The 3D geomechanics workflow is shown in Figure 15. This workflow proceeds from left to right on the diagram.

First, available data is reviewed and QCed, then rock physics modeling may be performed as appropriate. Then the workflow splits into two simultaneous tracks: the upper track is the 1D workflow just presented, in which correlations between well log properties and geomechanics properties and in situ stresses are established; along the lower track, a seismic volume is developed via QI workflows. The results of these two tracks are merged to produce 3D geomechanics volumes – geomechanics properties and in situ stresses – which may then be applied to field or well planning.

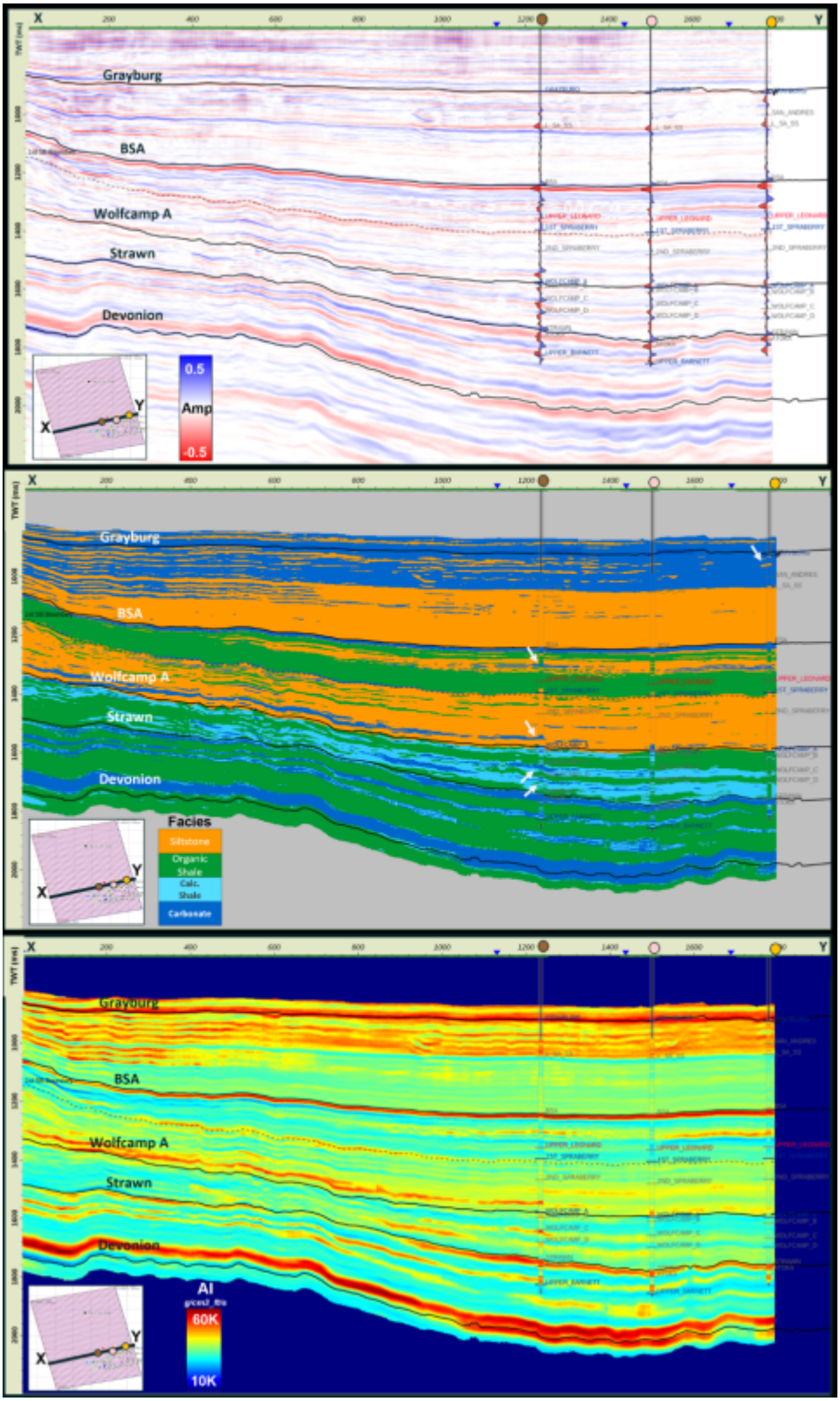

Figure 14. Seismic mid-angle stack (top), facies estimation (middle), and acoustic impedance from the inversion (bottom). All three are along the same inline shown in the bottom left corner. Corresponding synthetic traces, upscaled facies and impedance logs are a

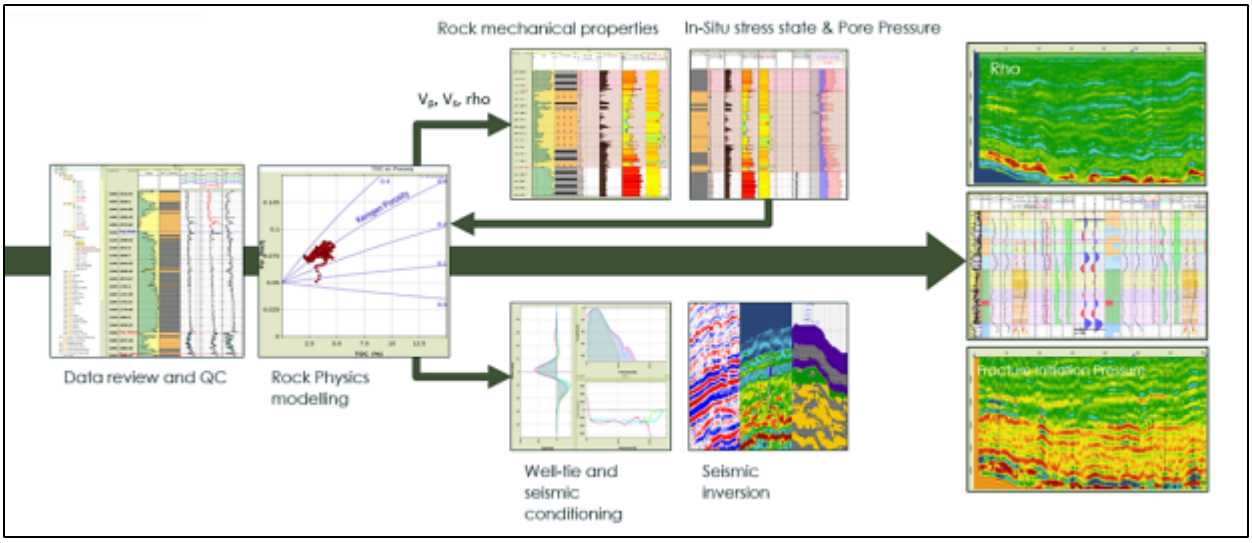

Figure 15. 3D Geomechanics workflow is shown. After initial data QC and rock physics modelling, the workflow splits into two simultaneous tracks: the upper track is the 1D workflow just presented, in which correlations between well log properties and geomechanics properties and in situ stresses are established; along the lower track, a seismic volume is developed via QI workflows. The results of these two tracks are merged to produce 3D geomechanics volumes – geomechanics properties and in situ stresses – which may then be applied to field or well planning.

3D volumes for pore pressure were generated using the established well-based models for Sv (vertical stress) and pore pressure prediction. Extracted pressure profiles from generated volumes show a good match with well-based predictions in blind test wells.

In the left image below of Figure 16, we are showing a cross section of the predicted pore pressure along the line highlighted in the insert. Note how pore pressure is increasing through the Wolfcamp and down towards the top of the Devonian. This is also illustrated by the two images to the right which shows the overpressure at top of the Wolfcamp (low) and at the base of the Wolfcamp (high). Note that the study area show lateral variation in overpressure magnitude (generally low on “platform”) and it would be interesting to investigate if there is any correlation between areas of low/high overpressure and production rates as has been observed in other areas of the Permian Basin.

Volumes of horizontals stress (Shmin, SHmax) were also produced using pore pressure and elastic properties from the inversion as input (Figure 17). Note how within Wolfcamp there are areas with a lot of layered heterogeneity leading to Shmin variability. This means that if you are going to stimulate in that area it potentially will lead to minimal vertical fracture height growth.

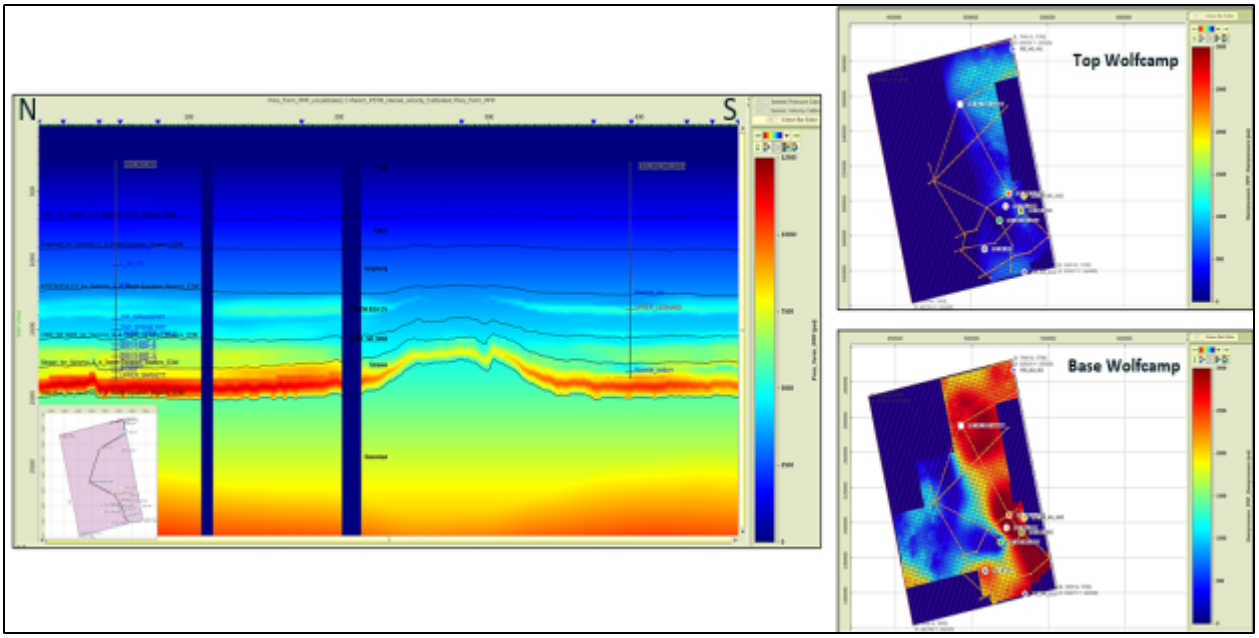

Figure 16. 3D volumes for pore pressure were generated for the study area using the established well-based models for Sv (vertical stress) and pore pressure prediction. In the left image is shown a cross section of the predicted pore pressure along the line highlighted in the insert. Note how pore pressure is increasing through the Wolfcamp and down towards the top of the Devonian. This is also illustrated by the two images to the left which shows that the overpressure at top of the Wolfcamp generally is low whereas it is at the base of the Wolfcamp. Also note that lateral variation in overpressure magnitude is indicated and it would be interesting to investigate if there is correlation between areas of predicted low/high overpressure and production rates as such a correlation has been observed in other parts of the Permian Basin.

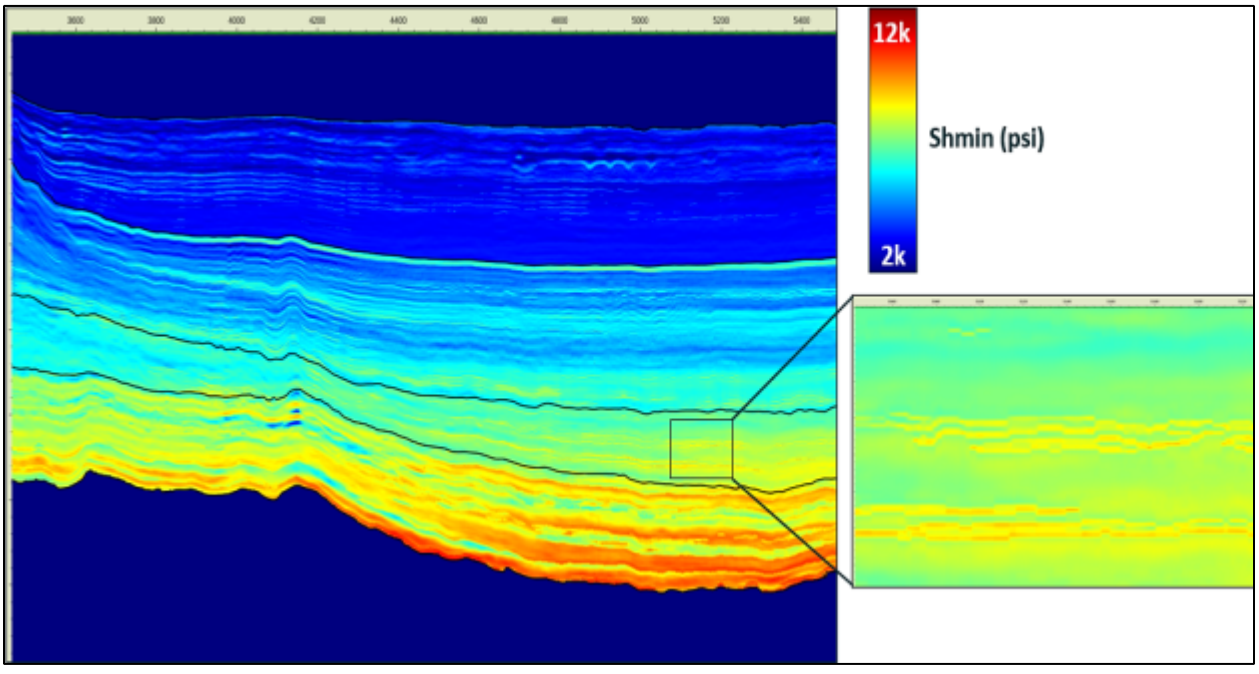

Figure 17. Section through Shmin volume created for the study area. Note how within Wolfcamp there are areas with a lot of layered heterogeneity leading to Shmin variability, which impacts vertical fracture height growth.

Conclusions

The elastic properties derived from seismic matched at all the blind tests. The derived calibrated geomechanical model was capable of reproducing geomechanical events, such as wellbore breakouts and DITF (drilling induced tensile fractures), reasonably well in blind test wells.

A 3D volume of pore pressure was constructed from a velocity volume and 3D geomechanical volumes were produced from pore pressure, Young's Modulus, Poisson's Ratio and vertical stress volumes. As the elastic properties are derived from Vp, Vs and Rho (property volumes from an inversion) this highlights the benefits of combining geomechanics and geophysical workflows likely resulting in improved KPIs such as drilling efficiency and potentially production rates and as such may impact future field development/planning.

Acknowledgements

We would like to thank Ikon Science, Fairfield Geotechnologies and Fasken oil & ranch for their support and permission for this study.

References

Anantharamu, V., Heller, J. and Gallop, J., 202. TOC removal methodologies for pore-pressure prediction in the organic-rich formations. In First International Meeting for Applied Geoscience & Energy (pp. 2308-2312). Society of Exploration Geophysicists.

Bhatnagar, P., Verma, S. and Bianco, R., 2019. Characterization of mass transport deposits using seismic attributes: Upper Leonard Formation, Permian Basin. *Interpretation*, 7(4), pp.SK19-SK32.

Friedrich, M. and Monson, G., 2013, Two Practical Methods to Determine Pore Pressure regimes in the Spraberry and Wolfcamp Formations in the Midland Basin. In: Unconventional Resources Technology Conference, Denver, Colorado, 12-14 August 2013.

Kemper, M. and Gunning, J. 2014. Joint impedance and facies inversion – Seismic inversion redefined. First Break, 32, no. 9, 89-95.

Lewis, A., Karr, B., Bianco, R. and Pollock, S., 2021, July. Illuminating Fine Scale Geology and Creating Robust Seismic Attributes Using High Trace Density Seismic Data in the Midland Basin. In SPE/AAPG/SEG Unconventional Resources Technology Conference.

Loughry, D. Epps, D., and Forrest, J., 2015, Using Pad ISIP, DFIT, and ESP Data to Generate a Pore Pressure Model for the Midland Basin. In: Unconventional Resources Technology Conference, San Antonio, Texas, 20-22 July 2015.

Luo, M., Baker, M., & Lemone, D. 1994. Distribution and generation of the overpressure system, eastern Delaware basin, western Texas and southern New Mexico. AAPG Bulletin, v.78, p.1386-1405.

Sinclair, Thomas Daniel (2007) The generation and continued existence of overpressure in the Delaware Basin, Texas, Durham theses, Durham University. Available at Durham E-Theses Online: http://etheses.dur.ac.uk/2289/.

Snee, J.E.L. and Zoback, M.D., 2018. State of stress in the Permian Basin, Texas and New Mexico: Implications for induced seismicity. The Leading Edge, 37(2), pp.127-134.

Swarbrick, R.E., 1995, Distribution and generation of the overpressure system, eastern Delaware Basin, western Texas and southern New Mexico: Discussion. AAPG Bulletin, v. 79, p. 1817-1821.

Van Der Loop, M., 2019, Paleo Overpressure in the Delaware Basin determined from DST, Resistivity and Mud Logs. In: AAPG Southwest Section Annual Convention, April 6-9, 2019, Annual Convention, Dallas, Texas.

Vernik, L. (2016) Seismic petrophysics in quantitative interpretation. Society of Exploration Geophysicists.

Xiong, Y., Winterfeld, P., and Wang Cong, 2015, Effect of Large Capillary Pressure on Fluid Flow and Transport in Stress-sensitive Tight Oil Reservoirs. In: SPE Annual Technical Conference and Exhibition, Houston, Texas, 28-30 September 2015.